CFD Validation for Hypersonic Flight: Hypersonic Double-Cone Flow Simulations

Graham V. Candler,* Ioannis Nompelis,** Marie-Claude Druguet†
Aerospace Engineering and Mechanics & Army HPC Research Center
University of Minnesota, Minneapolis MN 55455

Michael S. Holden,‡ Timothy P. Wadhams¶
Calspan-University at Buffalo Research Center, Buffalo NY 14225

Iain D. Boyd,§ Wen-Lan Wang**
Department of Aerospace Engineering
University of Michigan, Ann Arbor MI 48109

Abstract

At the 2001 AIAA Aerospace Sciences Meeting there was a blind comparison between computational simulations and experimental data for hypersonic double-cone and hollow cylinder-flare flows. This code validation exercise showed that in general there was good agreement between the continuum CFD simulations and experiments. Also, in general, there was good agreement between direct simulation Monte Carlo (DSMC) calculations and the experiments in regions of attached flow. However, in almost all of the computations, the heat transfer rate on the forebody of the cone was over-predicted by about 20%. The purpose of this paper is to report on our analysis of this difference. We perform CFD simulations of the hypersonic nozzle flow to assess the importance of vibrational nonequilibrium on the test conditions. We then recompute the flows using a new set of vibrational nonequilibrium conditions and consider the effects of a slip boundary condition at the model surface. Additionally, we analyze new heat transfer rate data on sharp and blunt 25° cones over a wider range of test conditions. This analysis appears to explain the discrepancy between the previous calculations and the experiments.

* Professor, AIAA Associate Fellow (candler@aem.umn.edu)
** Graduate Research Assistant, AIAA Student Member
† Research Fellow, also IUSTI-CNRS 6595, Marseille, France, AIAA Member
‡ Program Manager, AOEC, AIAA Associate Fellow
¶ Aeronautical Engineer
§ Associate Professor, AIAA Senior Member

Introduction

At the 2001 AIAA Aerospace Sciences Meeting, there was a session dedicated to a CFD code validation study. A number of computational researchers used their methods to predict the flow over several hypersonic configurations, and then the experimental data were revealed and compared to the computations. Two geometries were tested: a hollow-cylinder / flare that produces a weak viscous interaction, and a double-cone that produces a much more complicated flow field with a stronger viscous-inviscid interaction. The test conditions were chosen so that the free-stream conditions would be well characterized and the flows would be entirely laminar. Also to reduce the complexity of the computational analysis, nitrogen was used as the test gas.

This blind code validation study resulted in several key conclusions: First, the comparisons between the continuum computations and experiments were generally very good. For example, consider Fig. 1 which is taken from the paper of Harvey, Holden, and Wadhams.[1] The predicted surface pressure and heat transfer rate are plotted against the experimental data at two test conditions. Note that the pressure matches well on the cone forebody, through the separation zone, in the region of high pressure due to the shock-shock interaction, and on the second cone. Similarly for the heat transfer rate, with very good agreement in the separation zone, the shock interaction region, and on the second cone. The main differences are that the heat transfer rate on the cone forebody is over-predicted by about 20% and the separation zone is slightly too large, which results in the peak of pressure and heat transfer being too far downstream. The continuum computations by the other researchers showed essentially the same features, and additional calcula-

Report Documentation Page

Form Approved
OMB No. 0704-0188

1. REPORT DATE	2. REPORT TYPE	3. DATES COVERED
01 JAN 2006	**N/A**	**-**

4. TITLE AND SUBTITLE	5a. CONTRACT NUMBER
CFD Validation for Hypersonic Flight : Hypersonic Double-Cone Flow Simulations	5b. GRANT NUMBER
	5c. PROGRAM ELEMENT NUMBER
6. AUTHOR(S)	5d. PROJECT NUMBER
	5e. TASK NUMBER
	5f. WORK UNIT NUMBER
7. PERFORMING ORGANIZATION NAME(S) AND ADDRESS(ES) **Aerospace Engineering and Mechanics & Army HPC Research Center University of Minnesota, Minneapolis MN 55455**	8. PERFORMING ORGANIZATION REPORT NUMBER
9. SPONSORING/MONITORING AGENCY NAME(S) AND ADDRESS(ES)	10. SPONSOR/MONITOR'S ACRONYM(S)
	11. SPONSOR/MONITOR'S REPORT NUMBER(S)

12. DISTRIBUTION/AVAILABILITY STATEMENT
Approved for public release, distribution unlimited

13. SUPPLEMENTARY NOTES
See also ADM001860, Technologies for Propelled Hypersonic Flight (Technologies des vols hypersoniques propulses). , The original document contains color images.

14. ABSTRACT

15. SUBJECT TERMS

16. SECURITY CLASSIFICATION OF:			17. LIMITATION OF ABSTRACT	18. NUMBER OF PAGES	19a. NAME OF RESPONSIBLE PERSON
a. REPORT	b. ABSTRACT	c. THIS PAGE			
unclassified	**unclassified**	**unclassified**	**UU**	**14**	

tions at different flow conditions were generally similar to those described here.

A second conclusion of the study was that the hollow-cylinder / flare geometry computations also showed similarly good agreement with the experiments. However, in general all of the computations showed a small over-prediction in the heat transfer rate on the cylinder surface upstream of the separated flow region.

Comparisons between the experimental Schlieren images and the computed flow fields showed remarkably good agreement. The computations reproduced all of the visible features, including inflections in the bow shocks, separation shock locations, and shock interaction points. There is even evidence in the Schlieren of the predicted under-expanded jet that runs down the surface of the second cone.

Finally, the agreement between the Direct Simulation Monte Carlo (DSMC) calculations and experiments was not as good as the continuum calculations. Generally, DSMC is able to capture the surface pressure and heat transfer rate in the attached regions. However, in most cases, the DSMC calculations also over-predict the heat transfer rate on the cone and cylinder forebodies, as in the continuum calculations. DSMC apparently fails to predict the correct separation zone size for the massively separated flows, resulting in poor predictions of the flow in these regions. This is not surprising since the flows are characterized by a low Knudsen number, making them difficult to compute with DSMC.

In this paper, we focus on the main discrepancy between the computations and experiments, namely the over-prediction of the heat transfer rate on the cone and cylinder forebodies. We first evaluate how the free-stream conditions are inferred from the measured conditions during the experiments, and simulate the flow within the experimental facility nozzle. We are then able to predict the conditions of the experiment and determine the influence of vibrational nonequilibrium on the experimental conditions. Using these conditions, we then recompute the four cases that we considered in our previous paper and compare to experiments. These cases are Runs 28 and 35, which are sharp double-cones at Mach 9.5 and 11.3, and Runs 11 and 14, which are hollow-cylinder / extended flares at the same Mach numbers. We also perform the same analysis on new 25° cone heat transfer rate data from Holden.

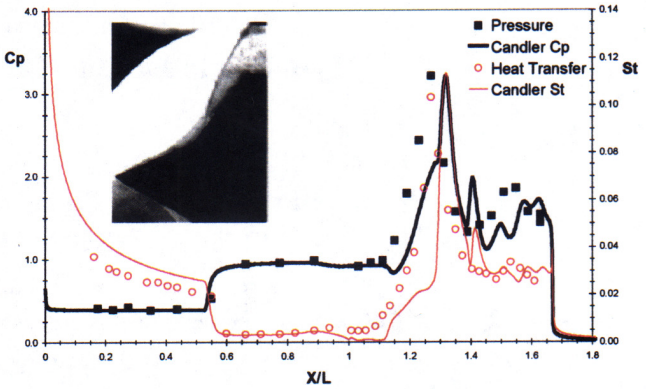

(a)

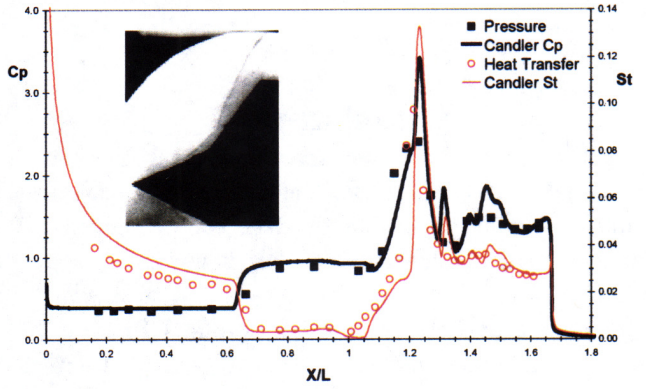

(b)

FIGURE 1. Normalized surface pressure and heat transfer rate for the sharp double-cone for (a) Run 28 ($M_\infty = 9.59$, $Re_\infty = 1.31 \times 10^5\,\mathrm{m}^{-1}$) and (b) Run 35 ($M_\infty = 11.30$, $Re_\infty = 1.33 \times 10^5\,\mathrm{m}^{-1}$) Computations by Candler *et al.*[2] Taken from Ref. 1.

Effect of Vibration on Test Conditions

One of the most important uncertainties in code validation is the specification of the free-stream conditions. This is particularly true in a hypersonic wind tunnel where high-temperature and pressure gas is expanded to a high Mach number. Non-ideal effects such as intermolecular force effects, chemical reactions, and vibrational excitation may affect the free-stream conditions. Additionally, it is not clear how one infers the test conditions from the quantities that can be measured in the test stream. In an impulse facility such as the shock tunnel used in the present experiments, the pressure and enthalpy in the reflected shock region are known. The test-section pitot pressure can be measured easily, and the heat transfer rate to a reference probe can also be measured.

In Holden's experiments, calibration runs are performed before the actual test conditions to verify the uniformity of the section flow. Then the tests are performed at the same nominal conditions as the cali-

bration. Additional pitot pressure measurements are made during the test to verify that the test conditions are consistent with the calibration run. To determine the free-stream conditions, a quasi-one-dimensional code is run using the measured post-reflected shock stagnation conditions as reservoir conditions. Because the effective area ratio of the nozzle is not known due to nozzle wall boundary layer displacement, the code is run to the point where the pitot pressure matches the measured pitot pressure. Then, the test conditions are taken to be those given by the quasi-one-dimensional code. This approach has been used successfully for a long time, but usually for air rather than nitrogen, and at higher pressures than considered in the present experiments.

It should be noted that in the hypersonic limit, the Rayleigh pitot pressure formula

$$\frac{p_{o2}}{p_\infty} = \frac{\gamma+1}{2} M_\infty^2 \left(\frac{\frac{\gamma+1}{2} M_\infty^2}{\frac{2\gamma}{\gamma+1} M_\infty^2 - \frac{\gamma-1}{\gamma+1}} \right)^{1/(\gamma-1)}$$

reduces to

$$\begin{aligned} p_{o2} &= \frac{\gamma+1}{2} \left(\frac{(\gamma+1)^2}{4\gamma} \right)^{1/\gamma-1} p_\infty M_\infty^2 \\ &= \frac{\gamma+1}{2\gamma} \left(\frac{(\gamma+1)^2}{4\gamma} \right)^{1/\gamma-1} \rho_\infty u_\infty^2, \end{aligned}$$

where p_{o2} is the measured pitot pressure and ∞ denotes free-stream conditions. Thus, the pitot pressure is simply a measurement of the kinetic energy per unit volume, or the axial-direction momentum flux.

Note that in an ideal adiabatic expansion to hypersonic conditions, we have

$$h_o = c_p T + \tfrac{1}{2} u^2 \simeq \tfrac{1}{2} u^2,$$

where we have assumed that $\frac{1}{2}u^2 \gg c_p T$. Thus given the reservoir enthalpy, we know the value of u^2 at all locations in the inviscid portion of the nozzle flow. Now, since the pitot pressure measurement gives us $\rho_\infty u_\infty^2$, all we have effectively measured is the free-stream density in an ideal expansion.

Now consider what happens if there is vibrational energy frozen in the flow during the expansion. We have

$$\tfrac{1}{2} u^2 = h_o - e_v^*,$$

where e_v^* is the vibrational energy per unit mass frozen in the flow. Thus for this non-ideal expansion, the kinetic energy will be lower than in an ideal expansion. And therefore, to achieve the same measured pitot pressure, the free-stream density will have to be larger.

Thus, we expect that the effect of vibrational freezing in the nozzle test-section is to lower the axial velocity and increase the density. We can show this more quantitatively if we numerically integrate an adiabatic flow while enforcing isentropic conditions from the reservoir conditions to the measured pitot pressure. The relevant equations are:

$$\begin{aligned} h_o &= h + \tfrac{1}{2} u^2 = \int_0^T c_p \, dT + \tfrac{1}{2} u^2 \\ ds &= c_p \frac{dT}{T} - R \frac{dp}{p} = 0 \end{aligned}$$

where c_p is a function of temperature. Using the reservoir conditions for Run 35 of $p_o = 547\,\text{psi} = 3.77\,\text{MPa}$ and $h_o = 4.12 \times 10^7\,\text{ft}^2/\text{sec}^2 = 3.83\,\text{MJ/kg}$, we compute an equilibrium reservoir temperature of $T_o = 3176\,\text{K}$ and density of $\rho_o = 3.998\,\text{kg/m}^3$. At these conditions, there is only a very small amount of dissociation, which is neglected.

If we then expand the reservoir gas to the measured pitot pressure of 0.541 psi using the above equations and assuming an equilibrium simple harmonic oscillator, we obtain the test-section conditions given in Table 1. If instead, we assume that the gas freezes at the throat temperature, we obtain a different set of conditions, also given in the table.

Note that in the above equation and in Table 1, the Mach number is computed with the frozen speed of sound. It should be noted that to obtain these results, we have used one additional piece of information, namely we must be able to compute the pitot pressure from the vibrational nonequilibrium conditions. We have performed CFD simulations of the flow over the pitot probes used in the experiments using a two-temperature, finite-rate relaxation model for nitrogen. These calculations show that under the conditions of interest, the Rayleigh pitot pressure formula gives the correct value of pitot pressure, p_{o2}. For example, the CFD simulation at the nonequilibrium

TABLE 1. Computed test-section conditions for Run 35 conditions using equilibrium and frozen flow assumptions. Adiabatic, isentropic expansion.

Case	Equilibrium	Frozen
T_∞ (K)	133.9	99.38
$T_{v\infty}$ (K)	133.9	2768
ρ_∞ (g/m^3)	0.548	0.612
u_∞ (m/s)	2716	2571
M_∞	11.51	12.65
$\rho_\infty u_\infty^2$ (Pa)	4044	4045
$\rho_\infty u_\infty^3$ (W/cm^2)	1098	1040

conditions given in Table 1 gives a pitot pressure of $p_{o2} = 0.541$ psi, which is the value obtained from the Rayleigh pitot pressure formula at these conditions.

This analysis of adiabatic, isentropic expansions with equilibrium and frozen vibration shows that for a given pitot pressure, vibrational freezing reduces the axial velocity and increases the density. We can estimate how this difference in the test-section conditions will affect the surface pressure and heat transfer. To first order, the surface pressure scales with $\rho_\infty u_\infty^2$, while the heat transfer rate scales with $\rho_\infty u_\infty^3$. Table 1 gives these quantities for the two conditions considered. Note that there is virtually no change in the dynamic pressure, as expected from the pitot pressure scaling argument given above. However, since the velocity is lower, the kinetic energy flux is reduced by 5.3%; this reduction will likely result in a lower heat transfer rate in the nonequilibrium case.

Nozzle Flow Simulations

The preceding analysis shows that vibrational freezing is likely to reduce the measured heat transfer rate. However, a more complete analysis is required to determine how much vibrational freezing occurs and to assess the additional non-ideal effects in the nozzle flow. Thus, we have performed a series of CFD simulations of the nozzle flows. We solve the axisymmetric compressible Navier-Stokes equations, along with a vibrational energy conservation equation. We allow finite-rate vibrational energy relaxation using Millikan and White rates.[3] Nitrogen dissociation and recombination is included with standard rate constants, but under the present conditions the dissociation levels are so low that they can be neglected. The Blottner curve-fits for viscosity[4] are used, and because the nozzle wall boundary layer is turbulent, we use the Baldwin-Lomax turbulence model.[5] A second-order accurate modified Steger-Warming flux vector splitting approach[6] is used, along with the Data-Parallel Line-Relaxation method.[7]

The nozzle grids are constructed directly from the CAD files of the nozzle contours. Typical grids use 1786 points in the axial direction and 128 points in the surface normal direction, with stretching at the surface. The nozzle throats are elongated, making the specification of the sonic line difficult. Thus the flow is computed from the constant diameter driven tube section, through the throat, and to the test-section. Thermo-chemical equilibrium was assumed at the inflow, and care was taken to specify the subsonic inflow conditions so that the total enthalpy is conserved in the computed flow.

Initial simulations of the nozzle flow were discouraging, with the centerline pitot pressure significantly over-predicted. This is caused by the turbulence model over-predicting the boundary layer displacement thickness in the nozzle exit plane. This may be a result of a deficiency in the turbulence model at high Mach numbers and low densities, or some other effect. Previous simulations of hypersonic nozzles showed significant variations in the computed test-section conditions depending on the choice of the turbulence model, with the Baldwin-Lomax model typically giving intermediate values for the boundary layer displacement thickness.[8] In any case, we were therefore forced to perform parametric studies where we allowed the flow to "relaminarize" (which is a fancy term for turning off the turbulence model) at different locations. This may not be completely arbitrary given that there is a very strong favorable pressure gradient and the test conditions are at a low density. With this approach, we were able to adjust the relaminarization location to match the measured displacement thickness for most of the test conditions.

For example, consider Fig. 2 which plots the measured pitot pressure for the Run 35 calibration run with the results of two nozzle simulations. Again, note that the fully turbulent calculation over-predicts the displacement thickness, resulting in a smaller effective area ratio and a larger pitot pressure. When the flow is assumed to relaminarize at 2.2 m from the throat (for a nozzle of just over 6 m in length), the displacement thickness matches the experiment much better. As a result, the computed pitot pressure agrees much better with the measurements.

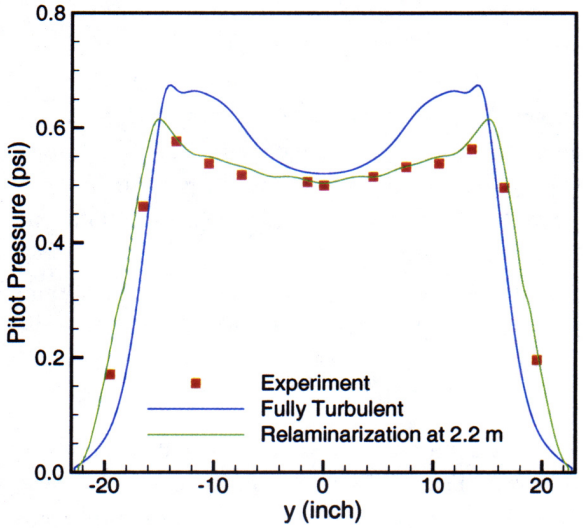

FIGURE 2. Run 1302 (calibration for Run 35) pitot pressure in the nozzle exit plane compared with axisymmetric nozzle computations.

With this relaminarization location, we then ran a nozzle simulation with the actual Run 35 reservoir conditions. The results of this simulation are tabulated in Table 2. The resulting dynamic pressure and kinetic energy flux are also given; note that the computed values are lower than the nominal conditions. This is a result of matching the experimental pitot pressure profile, rather than a single mean value. As a result, the computed value of $\rho_\infty u_\infty^3$ is 14% lower than the nominal conditions. It is also interesting to note the similarity in the results of the CFD calculations with the simple adiabatic and isentropic expansion. Note that the vibrational temperature freezes at slightly less than the throat temperature in the CFD simulation, which accounts for some of the differences in the two calculations.

A similar analysis was carried out for the other test conditions with similar agreement between the pitot pressure surveys and the computations. However, we were unable to obtain good agreement for the calibration run corresponding to Run 28. Figure 3 plots the exit-plane pitot pressure for this case. We have matched the boundary layer displacement thickness, but the radial variation of the pitot pressure is much larger in the computation than in the experiment. The reason for this is presently unknown, and as will be shown below, this is the only case for which this lack of agreement was obtained. Table 3 summarizes the computed free-stream conditions for the four cases considered.

TABLE 2. Nominal and computed test-section conditions for Run 35 reservoir conditions. CFD solution with relaminarization at 2.2 m from throat.

Case	Nominal	Nonequilibrium
T_∞ (K)	138.9	98.27
$T_{v\infty}$ (K)	138.9	2562
ρ_∞ (g/m^3)	0.5515	0.5848
u_∞ (m/s)	2713	2545
M_∞	11.30	12.59
$\rho_\infty u_\infty^2$ (Pa)	4059	3788
$\rho_\infty u_\infty^3$ (W/cm^2)	1101	964

TABLE 3. Nominal and computed nonequilibrium free-stream conditions for the 25-55° sharp double-cone and hollow-cylinder with extended flare flows.

Nominal	Run 11[a]	Run 14[a]	Run 28[b]	Run 35[b]
T_∞ (K)	128.9	156.1	185.6	138.9
ρ_∞ (g/m^3)	0.5066	0.7937	0.6545	0.5515
u_∞ (m/s)	2609	2432	2664	2713
M_∞	11.10	9.50	9.59	11.30
Nonequilibrium	**Run 11**	**Run 14**	**Run 28**	**Run 35**
T_∞ (K)	98.69	114.1	140.0	99.38
$T_{v\infty}$ (K)	2497	2269	2589	2768
ρ_∞ (g/m^3)	0.5866	0.7506	0.7372	0.6120
u_∞ (m/s)	2485	2327	2538	2571
M_∞	12.27	10.69	10.52	12.65

[a]Hollow-cylinder with extended flare
[b]Sharp 25-55° double-cone

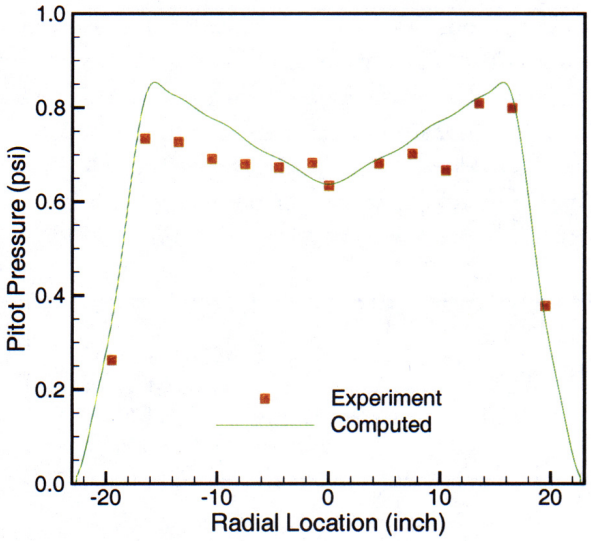

FIGURE 3. Run 1304 (calibration for Run 28) pitot pressure in the nozzle exit plane compared with axisymmetric nozzle computations.

Run 35 Analysis

With the test conditions predicted by CFD, we recomputed the test cases. Let us first focus on the forebody of the sharp double-cone at Run 35 conditions to see how the modified conditions affect the surface quantities. We use the same CFD code described above and in our previous work.[2] We use the results of the grid resolution studies that we performed in the past to select a grid that is certain to be fine enough to resolve the gradients in the tip region. For the first 5 cm of the tip, we use a grid of 260 × 256 points. We also performed DSMC calculations of this flow field, similar to those performed in Ref. 9.

Figure 4 plots the computed heat transfer rate and surface pressure based on the nominal Run 35 conditions and the nonequilibrium conditions computed with CFD. As expected because of the lower value of $\rho_\infty u_\infty^3$, the heat transfer rate is lower for the nonequilibrium test conditions. Our continuum results still over-predict the heat transfer rate by about 10%, and the DSMC results are generally higher still. The modified conditions produce a better agreement with the surface pressure, due to the lower free-stream dynamic

pressure predicted by the nozzle calculation (see Table 2). The source of the discrepancy between the CFD and DSMC calculations is not known. Interestingly, the computed surface pressures agree with one another very well, and thus it is likely that there is a difference in the effective surface energy exchange mechanism.

In our previous work, we considered the effects of a surface slip boundary condition. We found that there was some change in the predicted heat transfer, but not a significant level. However with the new free-stream conditions, we need to reconsider this issue because a substantial fraction of the energy is frozen in the vibrational energy modes. With the elevated vibrational temperature in the free-stream gas and the relatively slow relaxation of the gas within the flow field, it is possible that vibrational energy slip is important.

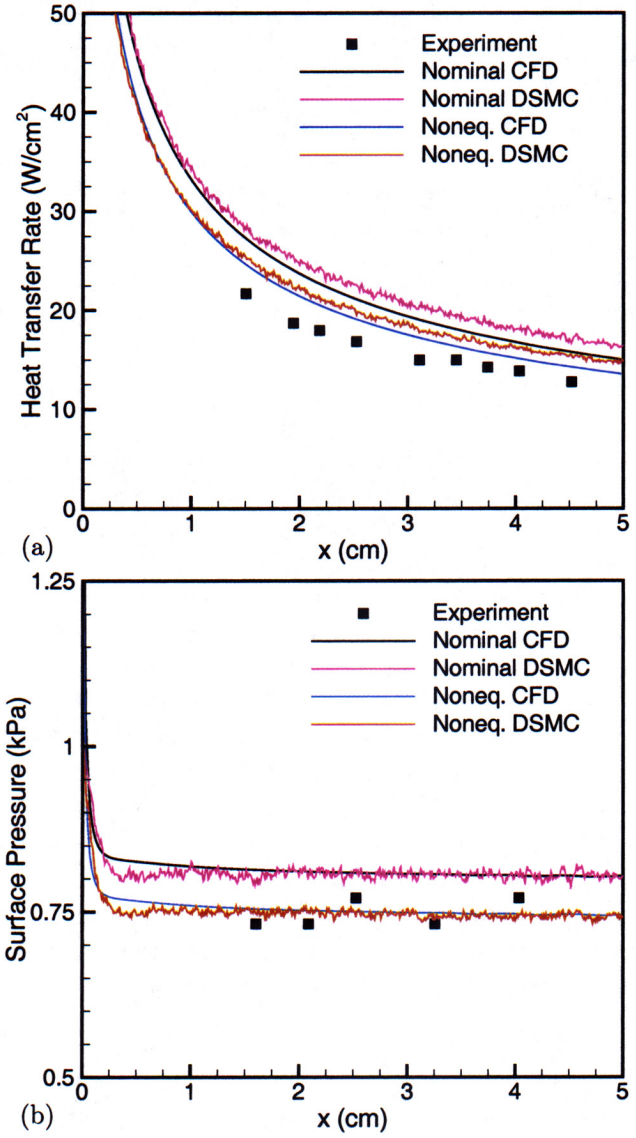

FIGURE 4. Heat transfer rate (a), and surface pressure (b) near the tip of the 25° cone at Run 35 conditions.

If we extend that standard Maxwell slip model to represent vibrational energy slip (or perhaps more commonly "jump"), we have

$$e_{v\,\mathrm{slip}} - e_{v\,\mathrm{wall}} = \frac{2-\sigma_v}{\sigma_v}\lambda_v \left.\frac{\partial e_v}{\partial n}\right|_{\mathrm{wall}}$$

where σ_v is the accommodation coefficient for vibration and λ_v is the mean-free-path that characterizes transport of vibrational energy. Because vibrational energy is independent of the translational energy modes in our model, we use the value of λ_v for the transport of momentum, namely $\lambda_v = 2\mu/\rho\bar{c}$, where $\bar{c}$ is the mean thermal speed of the gas, $\sqrt{8RT/\pi}$. This simple extension of the slip model is based on the work of Gokcen *et al.*[10] for example. The value of the vibrational energy accommodation coefficient is not well known, but previous calculations[11] have used values of σ_v as low as 0.1.

Figure 5 plots the computed heat transfer rate using this vibrational slip model with σ_v varied from 0.1 to 0.85. Also plotted is a simulation with no vibrational accommodation (an adiabatic surface condition for vibration). These calculations include momentum and temperature slip at the surface using the model of Gokcen,[10] and accommodation coefficients of 0.85. Clearly, the calculations predict a significant effect of vibrational energy slip on the heating rates. This is not surprising because at the nonequilibrium test conditions, 11% of the total energy is frozen in the vibrational modes. Note that there is very little change in the predicted heat transfer rate for $\sigma_v > 0.3$, and because of the uncertainty in the value of σ_v, we used a value of 0.5 for the remainder of the calculations.

These calculations show that the heat transfer rate to the tip of the cone is reduced by two effects. The vibrational modes of the gas freeze near the throat temperature, thereby reducing the test-section velocity. Secondly, due to the elevated vibrational temperature in the free-stream gas and the slow vibrational relaxation in the shocklayer, the effects of slip in vibrational energy at the surface are enhanced. Thus, much of the vibrational energy remains stored in the gas as it flows over the cone tip. This effect can be seen in Fig. 6, which plots the computed temperature profiles normal to the surface at axial location of 2 cm from the cone tip. Note that with the nominal free-stream conditions, there is essentially no vibrational excitation within shocklayer. But with nonequilibrium conditions, the vibrational temperature remains frozen except in the near-wall region. The effect of slip is also clear, with the vibrational temperature highly elevated at the surface for the slip boundary condition.

Based on these results, we performed CFD simulations of the entire double-cone flow field at the nonequilibrium Run 35 conditions. Figure 7 shows the computed translational-rotational temperature and vibrational temperature distributions in the flow field. Similar to Fig. 6, we see that the vibrational temperature remains frozen in the inviscid portion of the shocklayer. The gas is close to equilibrium in the separation zone because of its long residence time. The heat transfer rate results are plotted in Fig. 8. The modified test conditions and the surface slip model do not change the separation and reattachment locations, and as a result do not significantly alter the heat transfer to the second cone.

Figure 9 plots the computed pitot pressure near the nozzle exit plane at the Run 35 conditions. Because the contours are separated by only 0.025 psi, they accentuate the non-uniformities in the flow. But, there is variation in the flow properties on the scale of the model (diameter is 10 cm). Therefore, we extracted a line of data at the location where the model is located in the test section, and used this non-uniform data as upstream conditions for complete double-cone simulation. These results are plotted in Fig. 10. The non-uniform conditions reduce the size of the separation zone, and improve the agreement on the second cone. This excellent agreement may well be fortuitous, but it is clear that even a small level of non-uniformity in the free-stream conditions is important for this flow.

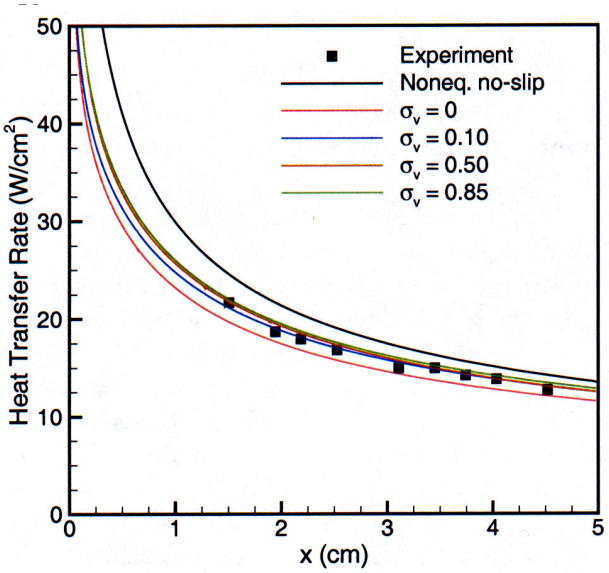

FIGURE 5. Variation of heat transfer rate on 25° cone with vibrational energy accommodation coefficient.

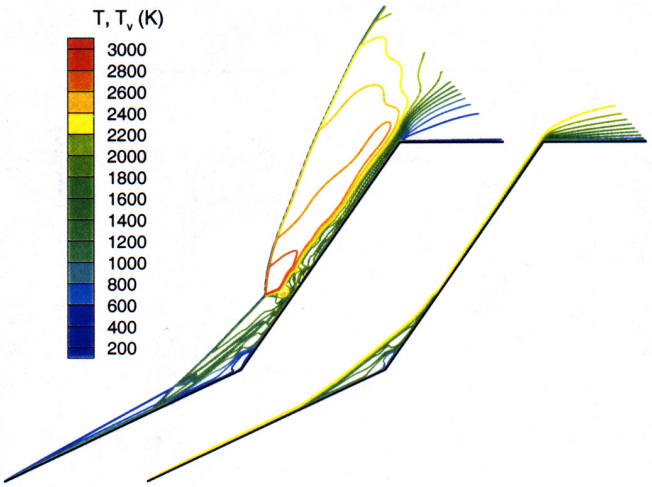

FIGURE 7. Temperature distributions in the flow field of Run 35 at nonequilibrium conditions.

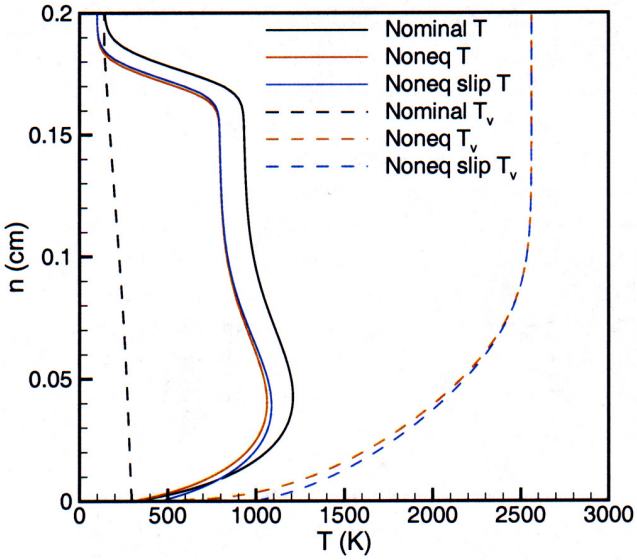

FIGURE 6. Temperature distribution normal to the surface at $x = 2.0$ cm.

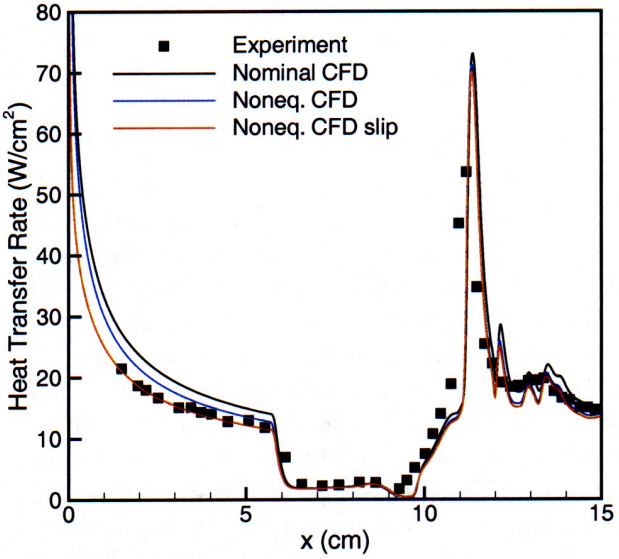

FIGURE 8. Heat transfer rate on the full double-cone at nominal and nonequilibrium Run 35 conditions.

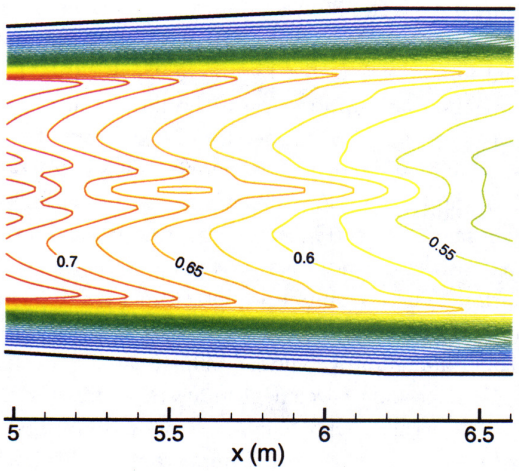

FIGURE 9. Pitot pressure contours (psi) in the test-section at Run 35 conditions.

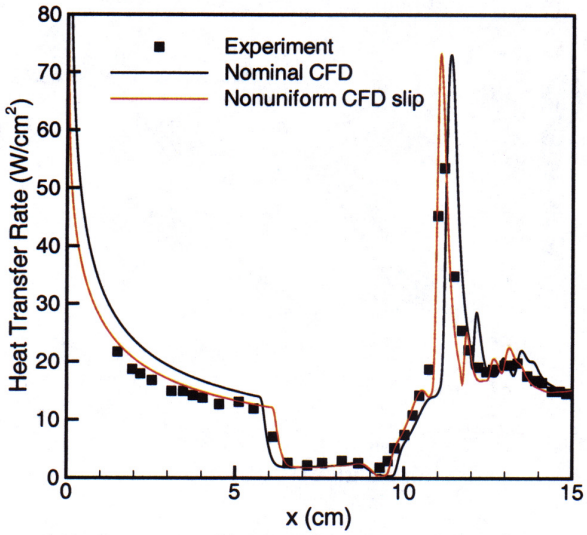

FIGURE 10. Heat transfer rate on the full double-cone with a non-uniform free-stream at Run 35 conditions.

FIGURE 10. Heat transfer rate on the full double-cone with a non-uniform free-stream at Run 35 conditions.

Run 28 Analysis

Figure 11 plots the computed heat transfer rate for the full double-cone at Run 28 conditions. The nonequilibrium test conditions result in a lower heat transfer rate near the cone tip that still slightly over-predicts the experimental data. However there is now a larger separation zone, which makes the agreement on the second cone worse than the previous results. Figure 3 showed that the nozzle simulation gave relatively poor agreement with the experiment pitot pressure survey. Thus, our predicted test conditions may still be in error for this case. It should be noted that Run 28 is the only case where such poor agreement was obtained, including eight new runs to be discussed below.

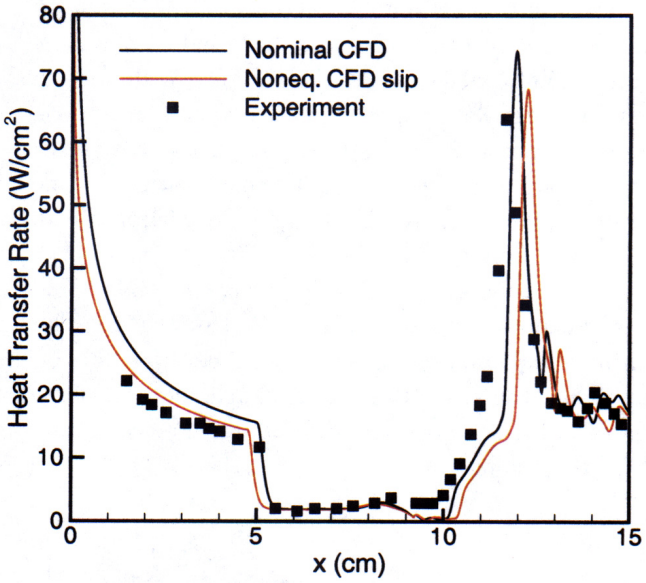

FIGURE 11. Heat transfer rate on the full double-cone at nominal and nonequilibrium Run 28 conditions.

New 25° Cone Data Analysis

Recently, Holden performed a new set of experiments designed to focus on the heat transfer rate to the forebody region of the 25° cone and on the cylindrical portion of the hollow-cylinder flare. Many different test conditions were run, with the total enthalpy varied from 2.41 MJ/kg to 3.72 MJ/kg; the stagnation pressure was also varied by a factor of about six, resulting in test-section densities varying by a factor of about 15. All runs were at the same nominal Mach number of 11.3. In contrast to the previous experiments, a pitot pressure survey was performed at the same time as the experiments so that additional calibration runs were not required. See Ref. 12 for more details on these new experiments.

We simulated the nozzle flows for the new experiments and obtained similar results to those discussed above. The level of agreement between the CFD simulations and the pitot pressure survey is illustrated in Fig. 12; generally there is a very good prediction of the boundary layer displacement thickness and pitot pressure variation. The nominal and predicted nonequilibrium test conditions are given in Table 4. Again, there is a substantial degree of vibrational nonequilibrium in the flows. However, in spite of the large variation in the reservoir conditions, the ratio of vibrational energy to the total energy of the test gas varies from only 8.1% in Run 12 to 10% in Run 25. Thus all of the runs have about the same level of nonequilibrium in the free-stream. Table 4 also gives the free-stream mean-free-path, λ_∞, which varies by a factor of 16 across the runs.

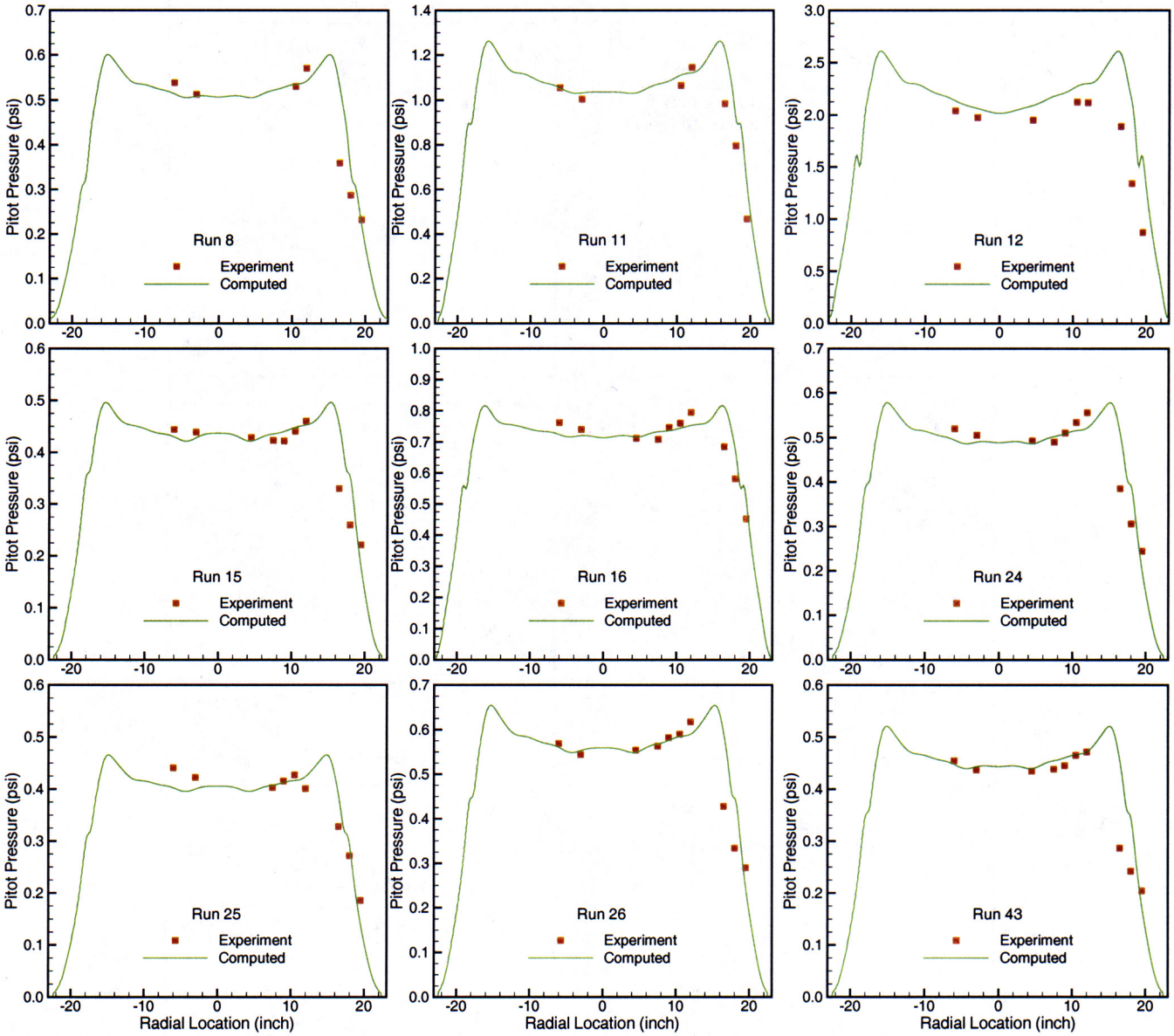

FIGURE 12. Pitot pressure in the nozzle exit plane compared with axisymmetric nozzle computations.

The results of the nozzle calculations were then used to simulate the flow over the 25° cone geometry. These calculations were "blind" in the sense that no attempt was made to go back and modify the predicted test conditions after the data were compared with experiments. Figure 13 summarizes the results. In all but one of the eight runs simulated, the nonequilibrium test conditions along with the slip boundary condition show a better agreement with the experiments. Run 12 is the exception, with a slight under-prediction of the heat transfer rate with the modified conditions. The importance of the slip modeling scales with the free-stream mean-free-path, λ_∞, which is tabulated in Table 4. Interestingly, the difference between the predictions using the two free-stream conditions also appears to increase with increasing λ_∞. This is consistent with vibrational nonequilibrium playing a larger role in the lower density and large mean-free-path flows.

Also plotted in Fig. 13 is a case with a blunt tip on the cone, shown as "Run 24 Blunt". In the case, the same cone geometry is used, but a 0.288 inch radius nose replaces the sharp cone tip. The CFD results for this case over-predict the heating rate for both conditions, even with the slip surface boundary condition. It should be noted that the measurements merge with one another at the last transducer location, indicating self-consistency in the data.

Overall, given the stated uncertainty in the reservoir conditions of approximately ±5%, the agreement for these widely varying test conditions is very encouraging.

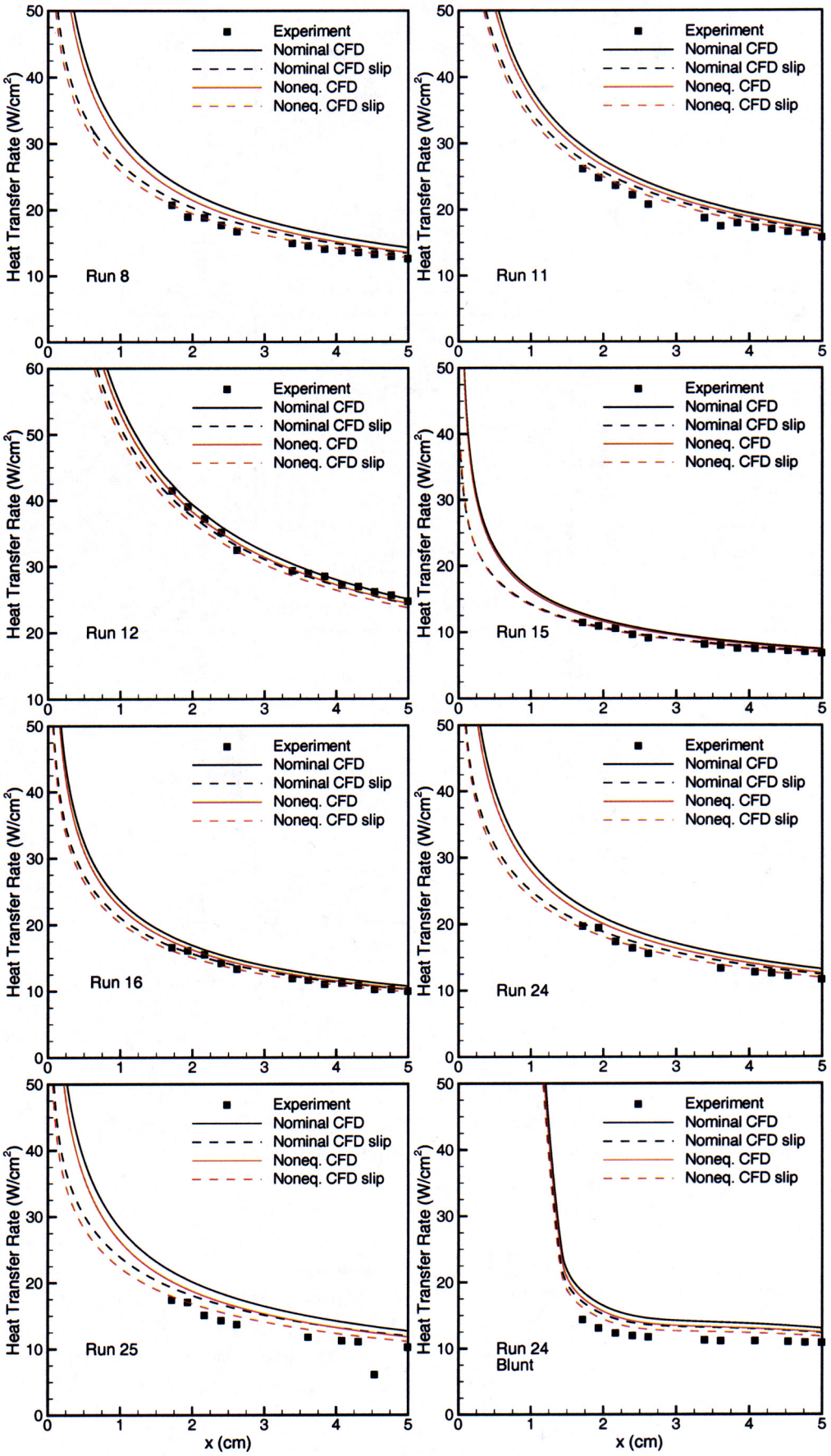

FIGURE 13. Heat transfer rate on the new 25° cone at nominal and computed nonequilibrium conditions.

TABLE 4. Nominal and computed nonequilibrium free-stream conditions for the new Holden experiments.[12]

Stagnation	Run 8	Run 11	Run 12	Run 15	Run 16	Run 24	Run 25	Run 26	Run 43
p_o (MPa)	3.741	8.236	17.43	3.123	5.747	3.600	2.841	4.127	3.233
h_o (MJ/kg)	3.716	3.335	3.437	2.406	2.601	3.567	3.613	3.456	3.400
Nominal	Run 8	Run 11	Run 12	Run 15	Run 16	Run 24	Run 25	Run 26	Run 43
T_∞ (K)	132.8	110.5	110.7	77.37	82.26	125.7	130.0	118.7	116.8
ρ_∞ (g/m^3)	0.5513	1.211	2.262	5.462	1.092	5.462	0.4550	0.6234	0.5044
u_∞ (m/s)	2675	2539	2579.0	2157	2243	2621	2636	2583	2560
M_∞	11.39	11.85	12.03	12.03	12.13	11.47	11.34	11.63	11.62
Nonequilibrium	Run 8	Run 11	Run 12	Run 15	Run 16	Run 24	Run 25	Run26	Run 43
T_∞ (K)	96.42	84.96	86.18	63.72	65.99	92.65	95.48	89.84	88.60
$T_{v\infty}$ (K)	2559	2286	2213	1895	1947	2491	2540	2421	2418
ρ_∞ (g/m^3)	0.5813	1.308	2.449	7.638	1.154	5.846	0.4804	0.6886	0.5563
u_∞ (m/s)	2549	2429	2477	2067	2153	2499	2511	2463	2441
M_∞	12.73	12.93	13.09	12.70	13.00	12.73	12.60	12.74	12.72
$\lambda_\infty(\mu$m)	116	51.2	27.4	8.64	57.3	11.5	140	97.5	121

Run 11 and 14 Analysis

In the previous study, hollow cylinder-flare geometries were also studied. We have performed an analysis of the effects of vibrational nonequilibrium and surface slip for two of these test cases, Run 11 and Run 14. The computed nonequilibrium test-section conditions are given in Table 3 above.

Figures 14 and 15 present the computed heat transfer rate and surface pressure distributions for these test cases. For Run 11, the nonequilibrium and slip increases the separation zone size beyond the already too large value for the nominal test conditions. For Run 14, the effect is reversed, but in this case the new conditions make the separation zone too small. In addition, the pressure in the separation zone is now under-predicted. But the heat transfer rate on the second cone is improved with the nonequilibrium conditions.

Thus, in general, the computed nonequilibrium conditions worsen the agreement between the computations and experiments. This lack of agreement is puzzling and we do not have an explanation for it at the present time. The modeling "improvements" that were successful for the cone should be applicable to this geometry at similar run conditions. Clearly, the hollow cylinder flow will have a larger slip effect than the cone; perhaps the present model is deficient under these high slip conditions. Flow non-uniformities may also play a role. However as we will see in the next section, the new experiments that Holden has run on the forebody of the hollow cylinder-flare geometry are more consistent with cone results.

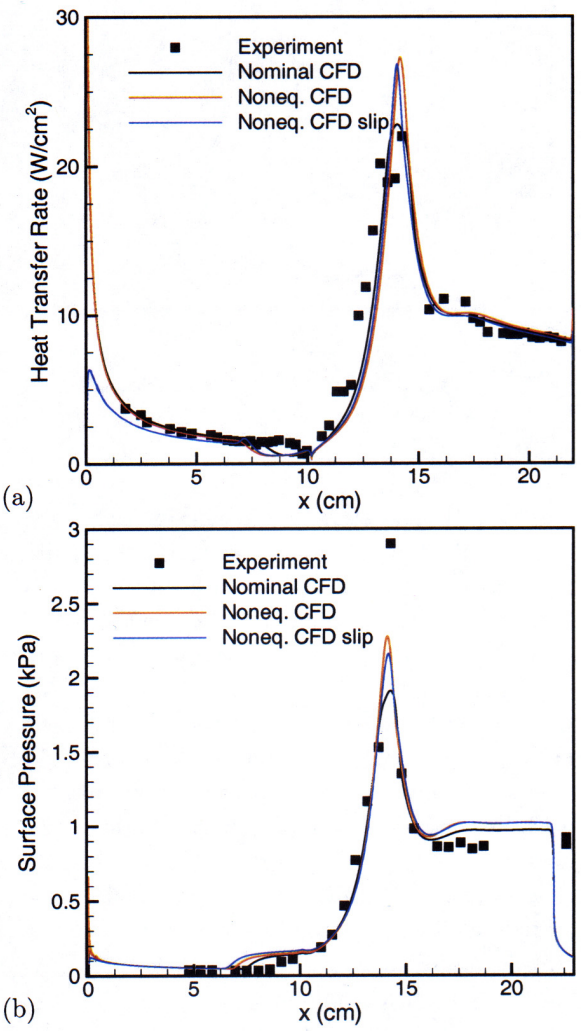

FIGURE 14. Heat transfer rate (a), and surface pressure (b) for the hollow cylinder-flare at Run 11 conditions.

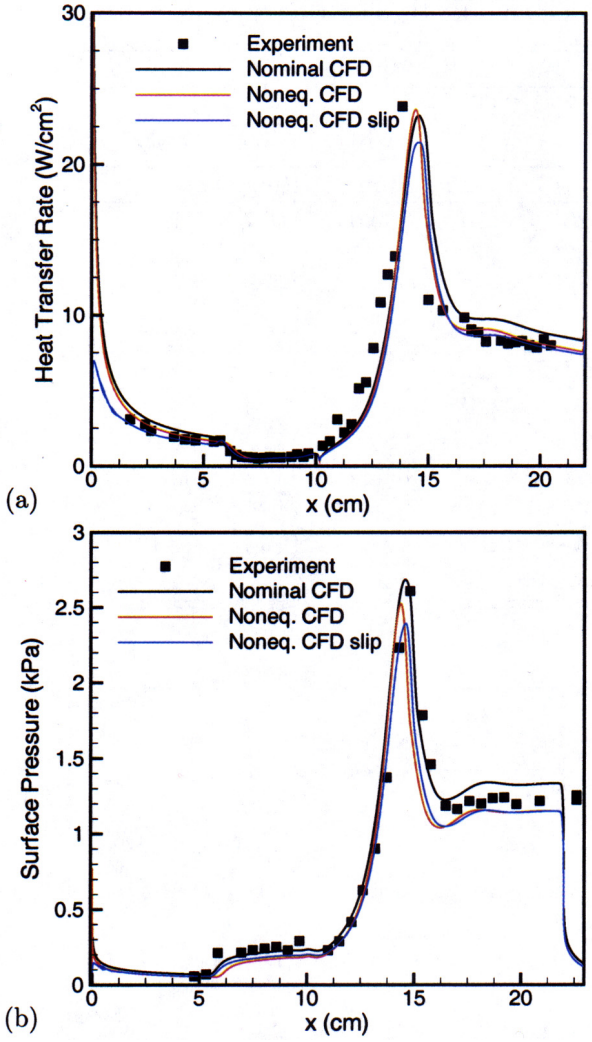

FIGURE 15. Heat transfer rate (a), and surface pressure (b) for the hollow cylinder-flare at Run 14 conditions.

New Hollow Cylinder Data Analysis

As mentioned above, Holden also performed a new series of runs on the forebody of the hollow cylinder-flare. This is similar to a flat plate flow without end effects. We have performed calculations at three conditions for the hollow cylinder: Runs 25, 26, and 43. The nominal and computed nonequilibrium conditions are given in Table 4 and the comparisons between the computed and measured pitot pressures are plotted in Fig. 12. Note the excellent agreement between the pitot pressure profiles, particularly for Runs 26 and 43. Run 25 is at similar conditions to the original hollow cylinder-flare at Run 11 conditions; the other two runs are at higher densities.

Figure 16 plots the surface pressure for the new hollow cylinder runs at Run 26 conditions, and Fig. 17 plots the surface heat transfer rate for Runs 25, 26 and 43. The first thing to note is that the pressure is significantly improved for all cases. Table 4 shows that relative to the nominal conditions, the nonequilibrium free-stream static pressure is 20% lower for Run 26. This results in a corresponding reduction in the surface pressure for the nonequilibrium conditions. For Run 25 and 43, the heat transfer rate prediction improves, and for Run 26 it is slightly too low. Again, the changes to the free-stream conditions and the effects of slip scale with the free-stream mean-free-path.

As with the new cone data, the agreement between CFD and computations is remarkable. This good agreement makes the lack of agreement with the previous hollow cylinder-flare data even more puzzling. For example, Run 25 is at essentially the same reservoir conditions as hollow cylinder-flare Run 11. But we have much better agreement with the new data. However, the new results are limited since they do not include the complex viscous-inviscid interaction at the cylinder-flare juncture.

Conclusions

This study has shown that the differences in the forebody heating and pressure seen in the previous code validation study are likely due to vibrational freezing in the nozzle and the failure of the no-slip boundary condition. Including these effects generally improves the comparison between the computations and experiments. But there are still several cases where the agreement is beyond the accuracy of the experimental data. Some more specific conclusions are:

1. It is important to assess the test-section conditions in hypersonic facilities using advanced diagnostics and CFD.

2. In hypersonic flows, the pitot pressure is proportional to $\rho_\infty u_\infty^3$. Because the effect of vibrational nonequilibrium is to lower the test-section kinetic energy, the density must increase for a given test-section pitot pressure. Since the heat transfer rate scales with $\rho_\infty u_\infty^3$, vibrational nonequilibrium tends to lower the heat transfer rate.

3. This effect is fully realized if the vibrational energy stays frozen in the gas as it passes over the model. The vibrational energy slip or jump at the surface decreases the energy transferred to the surface, and results in a sizable reduction in the heat transfer rate.

4. The importance of vibrational energy slip at the surface and vibrational freezing in the free-stream increase with increasing free-stream mean-free-path.

5. We have computed new nonequilibrium test conditions in the nozzles and found that by matching the displacement thickness at the nozzle exit plane, we can get very good agreement with measured pitot pressure profiles. As predicted, the nonequilibrium conditions

have lower axial velocity and higher density, with vibrational energy freezing near the throat conditions.

6. We have found essentially universal improvement in the sharp cone data for the old test conditions and for the widely varying new test conditions.

7. The DSMC calculations with the new test conditions show an improvement over the nominal conditions, but this improvement is less and the effects of slip are not as large. Therefore, there has to be a difference in the effect of the gas-surface interaction model between CFD and DSMC.

8. The old hollow cylinder-flare and new hollow cylinder runs show mixed results. For the old runs, the model improvements result in generally worse agreement with the experiments. However, for the new runs, the agreement is improved, especially for the surface pressure.

9. Clearly, CFD validation for hypersonic flows is not a simple task. There are so many exotic effects that take place in the experimental facilities and in flow fields, that it is not currently possible to say that CFD is "validated." That is an overly simple interpretation of a complex and subtle issue.

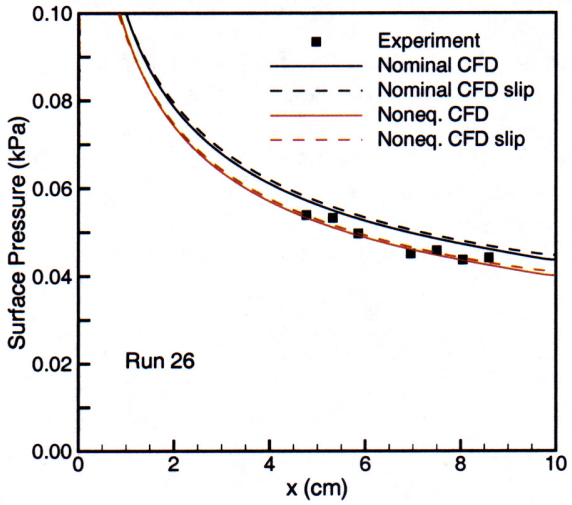

FIGURE 16. Surface pressure for the new hollow cylinder at Run 26 conditions.

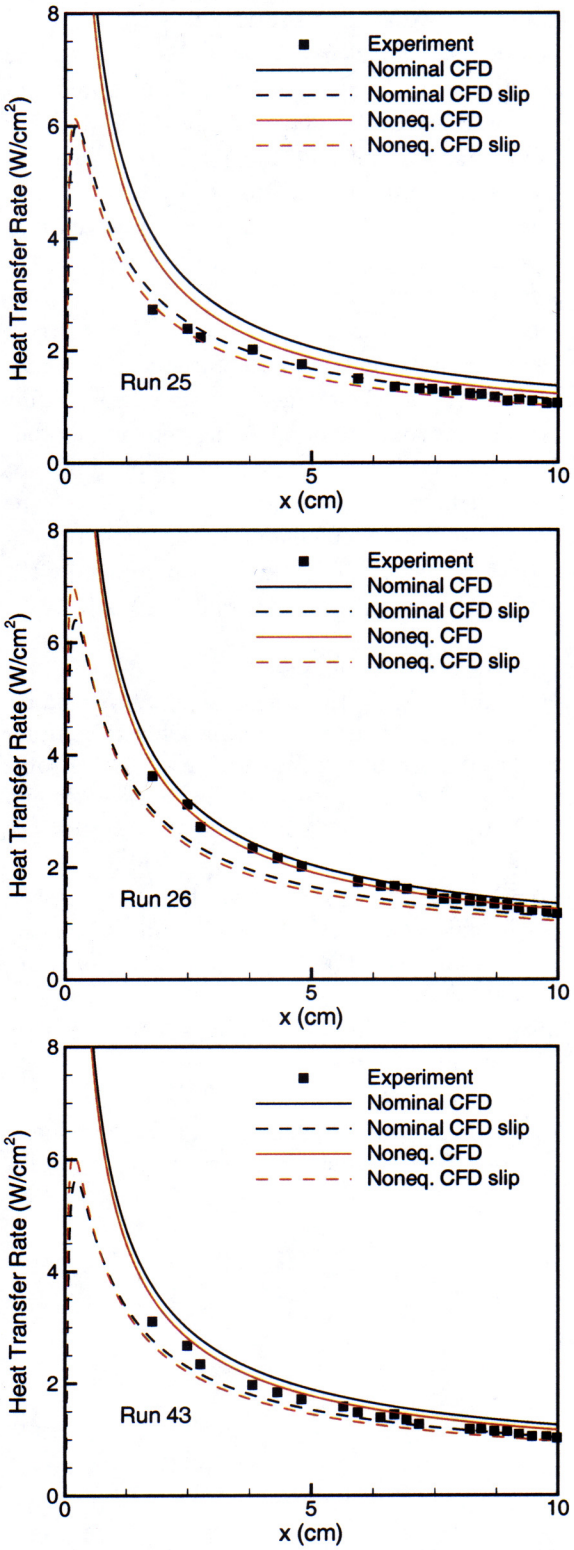

FIGURE 17. Heat transfer rate for the new hollow cylinder.

Acknowledgments

This work was sponsored by the Air Force Office of Scientific Research; at the University of Minnesota under grant F49620-01-1-0088 and at the University of Michigan under grant F49620-01-1-0003. The views and conclusions contained herein are those of the authors and should not be interpreted as necessarily representing the official policies or endorsements, either expressed or implied, of the AFOSR or the U.S. Government. This work is also sponsored by the Army High Performance Computing Research Center under the auspices of the Department of the Army, Army Research Laboratory cooperative agreement number DAAD191-01-2-0014, the content of which does not necessarily reflect the position or the policy of the government, and no official endorsement should be inferred. Part of the computer time was provided by the University of Minnesota Supercomputing Institute.

References

[1] Harvey, J.K., M.S. Holden, and T.P. Wadhams, "Code Validation Study of Laminar Shock/Boundary Layer and Shock/Shock Interactions in Hypersonic Flow, Part B: Comparison with Navier-Stokes and DSMC Solutions," *AIAA Paper No. 2001-1031,* Jan. 2001.

[2] Candler, G.V., I. Nompelis, M.-C. Druguet, "Navier-Stokes Predictions of Hypersonic Double-Cone and Cylinder-Flare Flow Fields," *AIAA Paper No. 2001-1024,* Jan. 2001.

[3] Millikan, R.C. and D.R. White, "Systematics of Vibrational Relaxation," *Journal of Chemical Physics,* Vol. 39, 1963, pp. 3209-3213.

[4] Blottner, F.G., M. Johnson, and M. Ellis, "Chemically Reacting Viscous Flow Program for Multi-Component Gas Mixtures," *Report No. SC-RR-70-754,* Sandia Laboratories, Albuquerque, New Mexico, 1971.

[5] Baldwin, B.S., and H. Lomax, "Thin Layer Approximation and Algebraic Model for Separated Turbulent Flows," *AIAA Paper No. 78-257,* Jan. 1978.

[6] Candler, G.V. and R.W. MacCormack, "The Computation of Hypersonic Ionized Flows in Chemical and Thermal Nonequilibrium," *Journal of Thermophysics and Heat Transfer,* Vol. 5, No. 3, pp. 266-273, July 1991.

[7] Wright, M.J., D. Bose, and G.V. Candler, "A Data-Parallel Line Relaxation Method for the Navier-Stokes Equations," *AIAA Journal,* Vol. 36, No. 9, pp. 1603-1609, Sept. 1998.

[8] Candler, G.V., and J.N. Perkins, "Effects of Vibrational Nonequilibrium on Axisymmetric Hypersonic Nozzle Design," *AIAA Paper 91-0297,* Jan. 1991.

[9] Boyd, I.D., and W.-L. Wang, "Monte Carlo Computations of Hypersonic Interacting Flows," *AIAA Paper No. 2001-1029,* Jan. 2001.

[10] Gökçen, T., *Computation of Hypersonic Low Density Flows with Thermochemical Nonequilibrium,* Ph.D. Thesis, Department of Aeronautics and Astronautics, Stanford University, June 1989.

[11] Boyd I.D., W.D. Phillips, and D.A. Levin, "Sensitivity Studies for Prediction of UltraViolet Radiation in Nonequilibrium Hypersonic Bow-Shock Waves," *Journal of Thermophysics and Heat Transfer,* pp. 38-44, Vol. 12, No. 1, 1998.

[12] Holden, M.S., and J.K. Harvey, "Comparisons Between DSMC and Navier-Stokes Solutions on Measurements in Regions of Laminar Shock Wave Boundary Layer Interaction in Hypersonic Flows," *AIAA Paper No. 2002-0435,* Jan. 2002.